



Development of time-varying global gridded T_s - T_m model for precise GPS-PWV retrieval

Peng Jiang^{1, 2}, Shirong Ye², Yin hao Lu¹, Yanyan Liu^{3, 2}, Dezhong Chen², Yanlan Wu¹

¹School of Resources and Environmental Engineering, Anhui University, Hefei, Anhui, China,

5 ²GNSS Research Center, Wuhan University, Wuhan, Hubei, China,

³Shenzhen Key Laboratory of Spatial Smart Sensing and Services, College of Civil Engineering, Shenzhen University, Shenzhen, Guangdong, China

Correspondence to: Peng Jiang (jiangpeng@ahu.edu.cn)

Abstract: Water-vapor-weighted mean temperature, T_m , is the key variable to estimate mapping factor between GPS zenith wet delay (ZWD) and precipitable water vapor (PWV). In near real-time GPS-PWV retrieving, estimating T_m from surface air temperature T_s is a widely used method because of its high temporal resolution and a fair degree of accuracy. Based on the T_m estimates and the extracted T_s parameters at each reanalysis grid node, analyses of the relationship between T_m and T_s were performed without smoothing of data which will produce superior results than other similar studies. Analyses demonstrate that T_s - T_m relationship has significant spatial and temporal variations. Then static and time-varying global gridded T_s - T_m equations were established and evaluated by comparisons with radiosonde data at radiosonde 758 stations in the Integrated Global Radiosonde Archive (IGRA). Results show that our global gridded T_s - T_m equations have prominent advantages than other globally applied models. Large biases of Bevis equation or latitude-related linear model at considerable stations are removed in gridded T_s - T_m estimating models. Multiple statistical tests at 5% significance levels show that time-varying global gridded model is superior to other T_s - T_m models at 83.64% of all radiosonde stations, while no model is significantly better at 5.54% of sites and others superior at only 10.82% of sites. GPS-PWV retrievals using different T_m estimates were compared at a number of IGS stations. By application of time-varying global gridded T_s - T_m equations, the relative differences of GPS-PWVs at most sites are within 1%. Such results are obviously superior to other T_s - T_m models. The differences between GPS-PWVs and radiosonde PWVs are influenced by other comprehensive factors instead of single T_m parameter. However evident improvements still exist at special site by using more precise T_s - T_m equations. PWV errors could decrease by more than 30% during wetter seasons.



1. Introduction

Water vapor is an important trace gas and one of the most variable components in the troposphere. Water vapor's transport, concentration and phase transition directly involve in atmospheric radiation and the hydrological cycle, leading to its key role in many climate change and weather processes (Song et al., 2016; Mahoney et al., 2016; Adler et al., 2016). It is always a challenge to measure water vapor content accurately and timely due to its small amount and high spatial-temporal variability. Several methods have been studied for decades, such as radio sounding, water vapor radiometer, sun photometers, GPS and others (Ciesielski et al., 2010; Perez-Ramirez et al., 2014; Li et al., 2016; Campmany et al., 2010; Liu et al., 2013). Compared with traditional water vapor observations, ground-based GPS water vapor measurement has advantages in high accuracy, high spatial-temporal resolution, all-weather availability and low-cost (Pacione and Vespe, 2008; Haase et al., 2003; Lee et al., 2010; Means, 2013; Lu et al., 2015). Therefore ground-based GPS water vapor products, mainly including precipitable water vapor (PWV) and slant water vapor (SWV), are widely used in many fields such as real-time vapor monitoring (Karabatic et al., 2011), weather and climate research (Van Baelen and Penide, 2009; Adams et al., 2017), numerical weather prediction (NWP) (Rohm et al., 2014) and so on. However, besides GPS observations, it requires some other kinds of meteorological elements to remotely sense PWV/SWV at each GPS station. Saastamoinen model is extensively adopted to compute zenith hydrostatic delay (ZHD), and surface pressure P_s is essential in the model equation (Saastamoinen, 1972). Then zenith wet delay (ZWD) is generated by deducting ZHD from zenith total delay (ZTD), and ZTD can be directly estimated from precise GPS data processing. Finally a conversion factor Π , which is used to map ZWD onto PWV, is determined by water-vapor-weighted mean temperature T_m over a GPS station. Mapping function from ZWD to PWV is expressed as (Bevis et al., 1992):

$$PWV = \Pi \cdot ZWD = \Pi \cdot (ZTD - ZHD) \quad (1)$$

and Π is computed using following formula:

$$\Pi = \frac{10^6}{\rho_w R_v [(k_3 / T_m) + k_2']} \quad (2)$$

where ρ_w is the density of liquid water, R_v is the specific gas constant for water vapor, $k_2' = (17 \pm 10) \text{K} \cdot \text{mbar}^{-1}$ and



$k_3 = (3.776 \pm 0.014) \times 10^5 \text{ K}^2 \cdot \text{mbar}^{-1}$ are physical constants (Sheng et al., 2013).

According to previous studies, error in T_m has significant influence upon the retrieval accuracy of PWV. The approximate
50 relationship between the relative error of PWV and T_m is (Wang et al., 2005):

$$\frac{\Delta PWV}{PWV} \approx \frac{T_m + \Delta T_m}{T_m} - 1 = \frac{\Delta T_m}{T_m} \quad (3)$$

There are three main approaches to estimate T_m , which have respective advantages and disadvantages, for different applications:

(1) Integral of vertical temperature and humidity profiles is believed to be the most accurate method. The profile data can
55 be extracted from radio sounding observations or NWP datasets (Wang et al., 2016). However, some inconveniences of this method have to be endured. It usually costs considerable time to acquire NWP data which normally have large volumes and be released every 6 hours beginning with 00:00 UTC every day. This limits the use of NWP data in near real-time GPS-PWV retrieving. The radiosonde data, which also provide accurate vertical atmospheric profile, have low spatial and temporal resolution. At most of radiosonde sites, sounding balloons are daily casted at 00:00 UTC and 12:00 UTC, furthermore lots of
60 GPS stations are not located close enough to any radio sounding site leading to no radiosonde data can be obtained for these stations most of time. Therefore such methods are appropriate for climate research or long-term PWV trends study but not meet real-time requirements.

(2) Several global empirical models of T_m are established based on analyses of T_m time series from NWP datasets or other sources (Chen et al., 2014; Yao et al., 2012; Bohm et al., 2015). T_m at any time and any location can be estimated from these
65 models independent of real meteorological observations. But some important real T_m variations, which maybe dramatic during some extreme weather events, can be lost without constraints of real data. So these modeled T_m estimates are not accurate enough for high-precise meteorological applications, such as providing GPS-PWV estimates for numerical weather predictions, etc.

(3) Many studies indicated that T_m parameter has evident relationships with some surface meteorological elements (e.g.
70 surface air temperature T_s). These surface meteorological parameters can be measured accurately and rapidly. T_m then is



estimated in real time using these surface measurements. For example, Bevis introduced Bevis T_s - T_m equation, $T_m=0.72 \times T_s+70.2$, according to analyzing 8712 radiosonde profiles collected at 13 sites in U.S. over two years(Bevis et al., 1992), and this equation has been widely used in many other studies.

According to Rohm’s research (Rohm et al., 2014), GPS-ZTD can be estimated very precisely by real-time GPS data processing. This means that T_m is a key parameter in near real-time GPS-PWV estimation. And method (3) is the most suitable means to estimate T_m in near real-time because of its balance between timeliness and accuracy. However, the relationship between T_m and T_s varies with location and time. Several regional T_s - T_m equations were established using profile data over corresponding fields (Wang et al., 2012). But it is not precise enough to apply the same T_s - T_m model in a vast field, e.g. in Indian region(Singh et al., 2014). Besides this, there are still vast areas, for example over the oceans, without high-precision specific T_s - T_m equations, and there exist large differences between the oceanic and terrestrial atmospheric properties. It is necessary to model T_s - T_m relationship over sea region, since several ocean-based GPS meteorology experiments were carried out and demonstrated the potential of such technique to retrieve PWV over the broad ocean (Rocken et al., 2005;Kealy et al., 2012). A global gridded T_s - T_m model has been established by smoothing T_m data from “GGOS Atmosphere” and T_s data from ECMWF reanalysis data in Lan’s study(Lan et al., 2016). The model, which has relative lower spatial resolution with $4^\circ \times 5^\circ$, however is statistic and the estimated T_m residuals due to time variations are not fixed (Yao et al., 2014a).

Table 1. Main differences between the T_s - T_m developed in this study and other global used T_s - T_m models

Strategies \ T_s - T_m Models	Bevis model (Bevis et al., 1992)	Latitude-related linear model (Yao et al., 2014b)	Global-gridded model (Lan et al., 2016)	Time-varying global gridded model (our study)
Applicable Regions	Regional/Global	Global	Global	Global
Data Sources	Radiosonde	T_s from $0.75^\circ \times 0.75^\circ$ ERA1, and T_m from $2^\circ \times 2.5^\circ$ “GGOS Atmosphere”	T_s from $0.75^\circ \times 0.75^\circ$ ERA1, and T_m from $2^\circ \times 2.5^\circ$ “GGOS Atmosphere”	T_s and T_m both from $0.75^\circ \times 0.75^\circ$ ERA1
Data Processing	Integrate radiosonde profiles	$4^\circ \times 5^\circ$ Sliding window smooth	$4^\circ \times 5^\circ$ Sliding window smooth	Integrate ERA-Interim profiles
Variations in model	Static without any variations	Spatial variations depend on only latitude(15° latitude interval), but no	$4^\circ \times 5^\circ$ global gridded, but no temporal variations	$0.75^\circ \times 0.75^\circ$ global gridded and considering



		temporal variations		time variations
--	--	---------------------	--	-----------------

The objective of this study is mainly to (1) develop global gridded T_s - T_m models without any spatial smooth of data and assess their precisions; and (2) study the performances of GPS-PWV retrievals using our T_s - T_m models. The main differences between the T_s - T_m developed in this study and other global used T_s - T_m models are listed in Tab. (1). In section 2 the data sources and T_m determining methods are introduced in detail. Then in section 3 we analyze the T_s - T_m relationships and their variations on a global scale. Global-gridded T_s - T_m estimating models in different forms are established and evaluated in Section 4. Section 5 compares different PWV retrievals and Section 6 presents conclusions based on our experiments.

2. Data Sources and Methodology of T_m Determination

2.1 T_m Definition

T_m is defined as a function related to temperature and water vapor pressure. It can be approximated as following formula(Bevis et al., 1992):

$$T_m = \frac{\int \frac{e}{T} dz}{\int \frac{e}{T^2} dz} \approx \frac{\sum_{i=1}^n \frac{e_i}{T_i} \Delta z_i}{\sum_{i=1}^n \frac{e_i}{T_i^2} \Delta z_i} \quad (4)$$

where e and T respectively represents vapor pressure in hPa and temperature in Kelvin, i denotes the i th pressure level and Δz_i is the height difference of i th levels. Vapor pressure e is calculated using equation $e=e_s \times RH$, RH is the relative humidity and saturation vapor pressure e_s can be estimated from temperature observations using Goff-Gratch formula (Sheng et al., 2013). The integral intervals are from the earth surface to the atmospheric top.

2.2 Data sources and Methodology of T_m Determination

Equation (4) needs temperature, height and relative humidity values of several atmospheric levels through the entire atmosphere. These essential profile data can be obtained from radiosonde or NWP datasets.

We employed radiosonde data from Integrated Global Radiosonde Archive (IGRA,



<ftp://ftp.ncdc.noaa.gov/pub/data/igra>) to calculate T_m . Version 2.0 of the IGRA-derived sounding parameters provides pressure, geopotential height, temperature, saturation vapor pressure and relative humidity observations at observed levels. Bias maybe introduced if integrals were terminated at lower levels(Wang et al., 2005), so the integrals were performed up to the topmost valid radiosonde data. According to our quality control processes some radiosonde profile data were rejected. Surface observation must be available, and top profile level should not be lower than 300 hPa standard level. Furthermore the level number between surface and top level is required to be greater than five levels to avoid too sparse vertical profile. At most radio sounding stations, sounding balloons are launched every 12 hours, and their ascending paths are assumed to be vertical.

Profile data including same elements are usually provided by NWP products at certain vertical levels. ERA-Interim from ECMWF, provides data on a regular 512 longitude by 256 latitude N128 Gaussian grid after the grid transforming performed by NCAR's Data Support Section (DSS). On each grid node of ERA-Interim, temperature, relative humidity and geopotential at 37 isobaric levels from 1000 hPa to 1 hPa can be obtained. Dividing the geopotential by constant gravitational acceleration value ($g \approx 9.80665 \text{ m/s}^2$), we can determine the geopotential heights of surface and levels. Datasets are available at 00:00, 06:00, 12:00 and 18:00 UTC every day and has been covering a period from 1979.01 to present.

In theory, the computation of Eq. (4) should be operated through the entire atmosphere and geopotential height should be converted to geoid height. However, vast majority of the water vapor concentrate at the troposphere, moreover the geopotential heights of top pressure levels in the two selected reanalysis datasets are around 30~40 km. Geopotential height is very close to geoid height in such height range. According to our computation, relative difference between them with only 0.1%~0.9%. In fact, the height difference Δz can be replaced by geopotential height difference Δh in Eq. (4), since the division operation can almost eliminate the difference between two different height types. The value change of T_m attributed to the height replacement will extremely approximate to zero. For convenience of calculations, we directly employed geopotential height variable of reanalysis datasets to estimate T_m . In this paper, we denoted the T_m derived from ERA-Interim as T_{m_ERA-I} .

At each model grid node of reanalysis data, the computation of Eq. (4) starts from the surface height to the top pressure level. Therefore the pressure levels below surface height were rejected in calculation. Near-ground air temperature T_s is defined as the variable of “temperature at 2 meters above ground”, and surface water vapor pressure can be derived from “2 meter



dewpoint temperature” variable in ERA-Interim. These T_s were also used in the regression analyses between T_m and T_s in following study.

3. Correlation between T_s and T_m

Many studies have indicated the close relationship between surface air temperature T_s and weighted mean temperature
135 T_m . However, T_m is also found to be not closely related to T_s in some other regions, e.g. in Indian zone (Raju et al., 2007). Using T_m and T_s generated from global gridded reanalysis data, we are able to study the relationship between T_s and T_m in detail.

We first carried on linear regression analyses on the four years long T_s and T_m data generated from point radiosonde data and global gridded ERA-Interim datasets. Analysis results are shown in Fig. (1). Although two datasets have different temporal resolutions (12 hours for radiosonde data and 6 hours for ERA-Interim data) and spatial resolutions, both analyses agree very
140 well with each other. Our analyses also indicate that correlation coefficients between T_s and T_m are generally related to point’s latitude as well as other studies (Yao et al., 2014b). Significant positive correlation coefficients can be found in mid- and high latitudes, and reaches the maximum in Polar Regions. Then the correlation coefficients drop dramatically in low latitudes. We further analyzed the main reason for such change. T_m variable in low latitudes is stable and shows its independence of other parameters. To study the variations of T_s and T_m , we illustrated denary logarithm values of their standard deviations in Fig. (2).
145 It is evidently that T_m varies much less in low latitudes. However, besides latitude-related features, it is worth noting that there are obvious T_s - T_m correlation coefficient differences between lands and oceans. Analyses even demonstrate negative correlation coefficients over certain oceans, e.g. low-latitude Western Pacific, Bay of Bengal or Arabian Sea. It may be mainly attributed to the different thermodynamic properties of underlying surface, including the transfer of water latent heat, the different specific heat capacities, etc. These properties influence the T_s greatly, leading to the significantly smaller variations
150 of T_s over the seas than over the lands. Unreliable regression analysis results may be derived by the T_s and T_m both with small variations. In Fig. (3), scatter plots of T_s and T_m from ERA-Interim datasets at two locations N 0.35° E180.00° and N70.53° E180.00° are given. Compared with the other point, the T_s - T_m relationship at the point near the equator, as the blue dots show, is quiet obscure since the whole variation ranges of T_s and T_m are both below 10 K. The linear regression result, as the magenta



line shows, also makes less sense with low T_s - T_m correlation coefficient of only -0.0893. Besides complicated spatial variations,
155 researches have revealed that T_s - T_m relationships also have temporal variations(Wang et al., 2005). So a good T_s - T_m model
should take both spatial and temporal variations into consideration, which is the main work in the following sections.

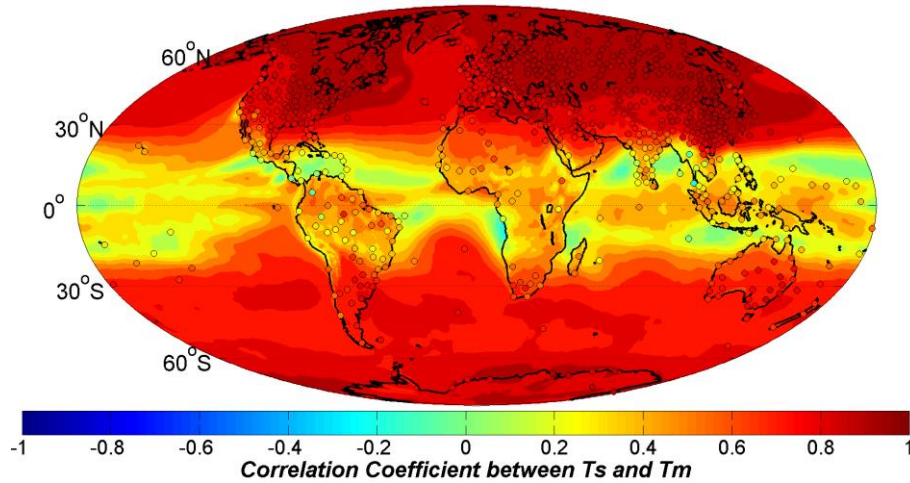
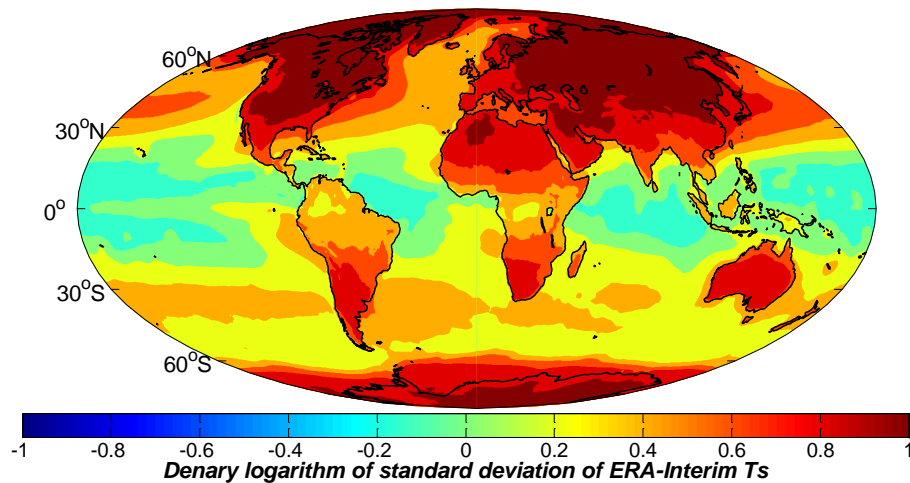


Figure 1: Correlation coefficients between T_s and T_m generated from radiosonde data (dots) and ERA-Interim reanalysis datasets (color-filled contours) over a period of 4 years from 2009 to 2012.

160



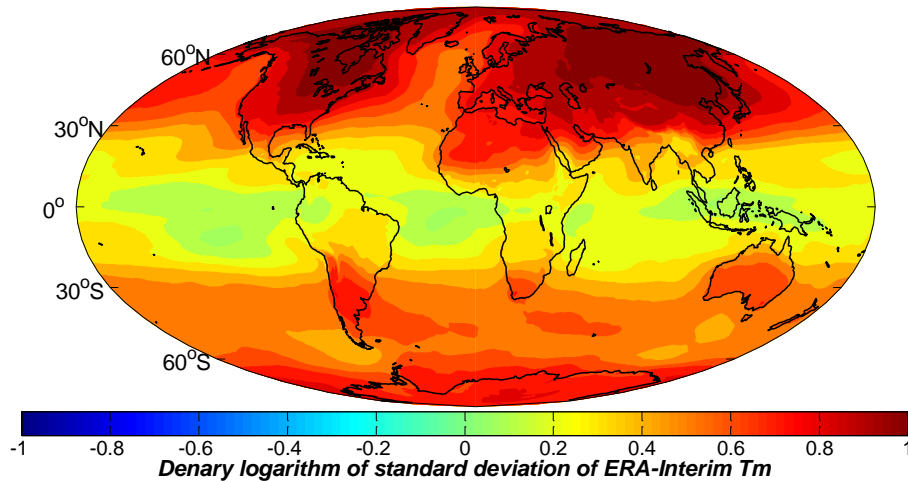


Figure 2: Denary logarithm of standard deviation of (top) T_s and (bottom) T_m generated from (left) NCEP FNL and (right) ERA-Interim reanalysis datasets over a period of 4 years from 2009 to 2012

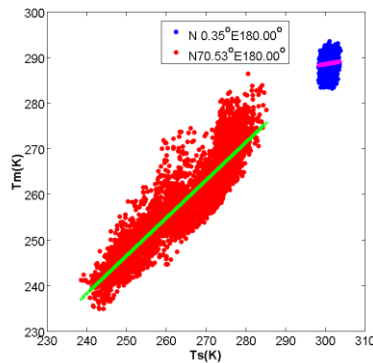


Figure 3: T_s - T_m scatter plots at two locations: (blue dots) $N 0.35^\circ E180.00^\circ$ and (red dots) $N70.53^\circ E180.00^\circ$, the magenta and green lines are their linear fitting curves

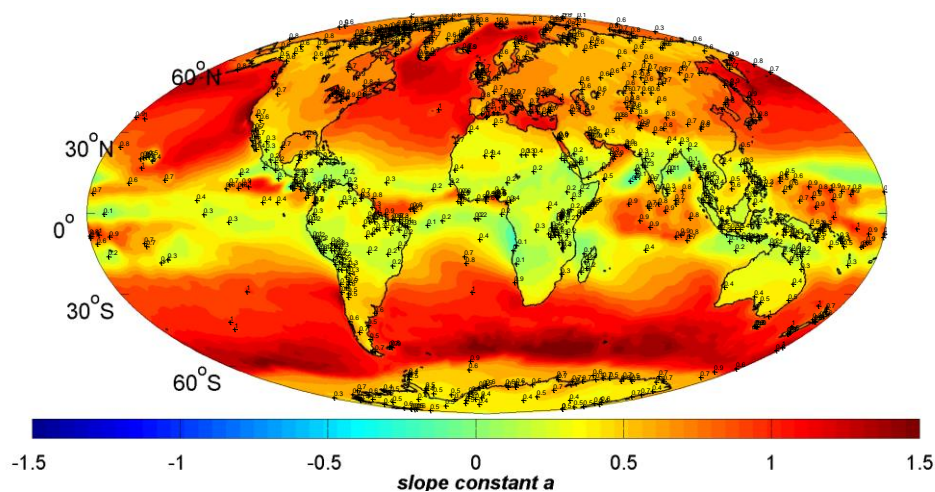
4. Developments of Global-gridded T_s - T_m models

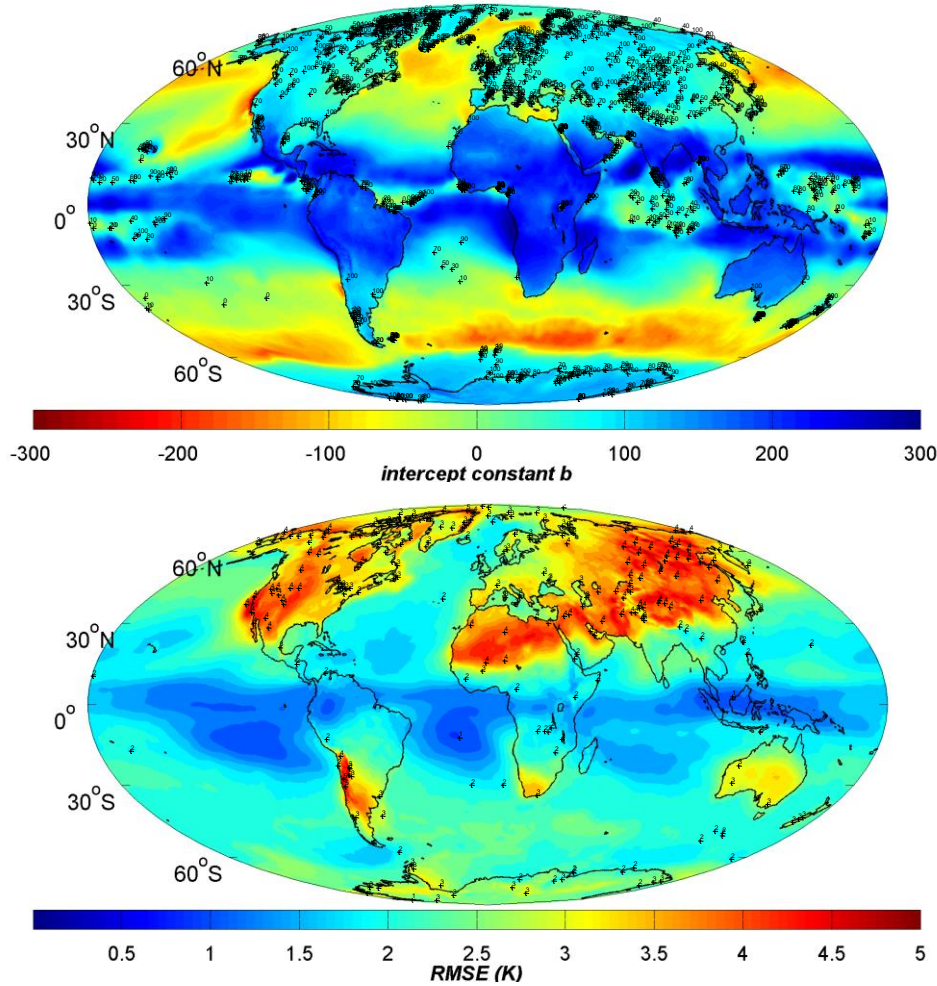
Since T_s - T_m relationship has complicated spatial variations, it is necessary to establish detailed global gridded T_s - T_m estimating equations for precise GPS-PWV remote sensing. In this section, static and time-varying global gridded T_s - T_m models are established and assessed.

4.1 Static global-gridded T_s - T_m model



Linear formulas including T_s and T_m , which is expressed as $T_m = a \times T_s + b$, are adopted in most studies, such as Bevis
equation. Based on the T_s and T_m products from ERA-Interim reanalysis datasets, we performed linear fittings of T_s versus T_m
175 on each grid point. Then slope constant (a) and intercept constant (b) of each linear expression and fitting RMSEs were
calculated and contoured in Fig. (4). The a and b values are related to point's latitude as well as its underlying surface. Constant
 a value varies from 0.6 to 0.8 when constant b about 100~50 over most continents in northern mid-high latitudes. The constants
in Bevis equation, which are 0.72 and 70.2 respectively, are within such value ranges. Constant a is smaller (about 0.5~0.7)
over lands in the southern mid-high latitudes. Specially, there are acute value changes of constant a and b from lands to seas
180 in mid-high latitudes. The reason is the different variation features of surface air temperature while there are not much
differences of T_m variations between seas and lands, which can be seen in Fig. (2). In low latitudes, the a value is smaller than
other regions whether over lands or oceans because of the low T_s and T_m variations. Fitting RMSEs are within 2~4 K over mid-
high latitude lands, and relative lower values over the seas or low latitude areas. The reason for the low RMSE values over the
oceans around equator is just the smaller fluctuations of T_m . Attributed to no spatial or temporal smooth of any data in our
185 study, the precision and resolution of our static model, with no RMSE larger than 4.5 K, is clearly better than previous studies.
(Lan et al., 2016).





190 **Figure 4: Distribution of (top) slope constant a , (middle) intercept constant b , and (bottom) RMSE of static linear T_s - T_m equations at ERA-Interim grid nodes.**

4.2 Time-varying global-gridded T_s - T_m model

T_s - T_m relationship has time variations which should also be considered in precise T_s - T_m model. Therefore a time-varying equation is applied for T_s - T_m regression at each grid node:

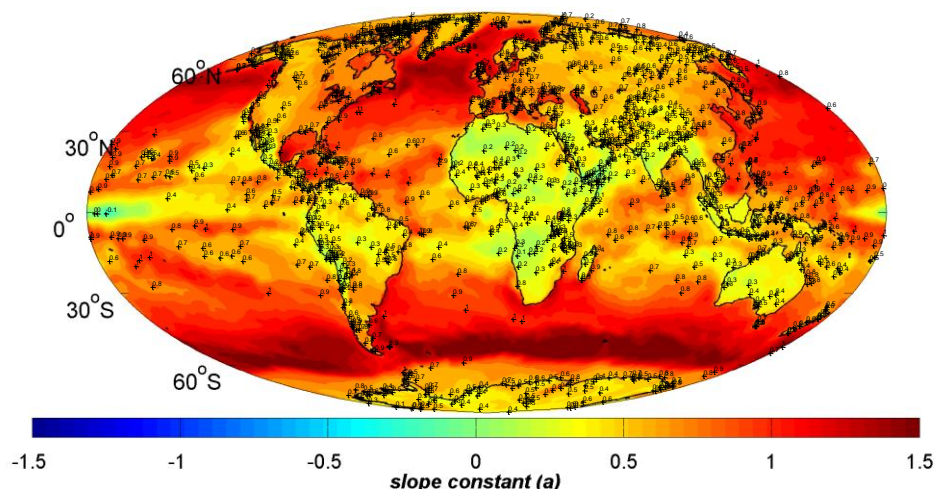
$$\begin{aligned}
 T_m = & a \times T_s + b + m_1 \cos\left(\frac{\text{doy}}{365.25} \cdot 2\pi\right) + m_2 \sin\left(\frac{\text{doy}}{365.25} \cdot 2\pi\right) + n_1 \cos\left(\frac{\text{doy}}{365.25} \cdot 4\pi\right) + \\
 & n_2 \sin\left(\frac{\text{doy}}{365.25} \cdot 4\pi\right) + p_1 \cos\left(\frac{\text{hr}}{24} \cdot 2\pi\right) + p_2 \sin\left(\frac{\text{hr}}{24} \cdot 2\pi\right)
 \end{aligned} \quad (5)$$

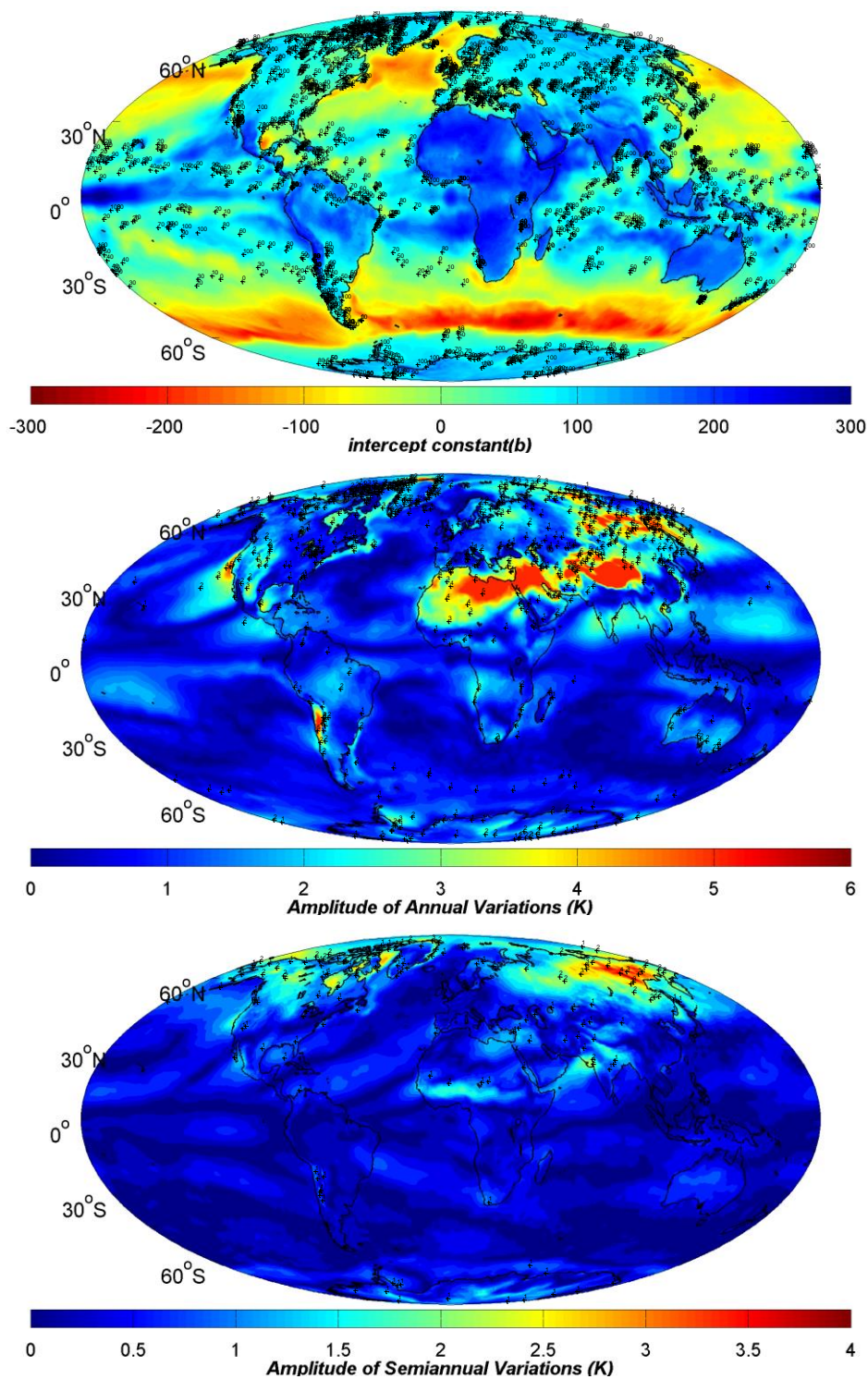
195



where doy represents the observed day of year and hr is the observed hour in UTC time; (m_1, m_2) , (n_1, n_2) and (p_1, p_2) are the fitting coefficients of formula items to reflect T_s-T_m relationship's annual, semiannual and diurnal variations.

Our regression indicated that the static terms in Eq. (5), which are determined by coefficients a and b , are similar to the static models in section 4.1 expect a little differences over some oceans. Besides a and b , we also illustrated the amplitudes of annual, semiannual and diurnal terms. We can see that there are large annual variations (amplitude > 5 K) in the vast regions from Tibet to North Africa, and some places in Siberia and Chile, while diurnal variations (amplitude > 3 K) mainly occurs in mid-latitude lands such Northeast Asia or North America. Semiannual variations, however, are small in most areas expect some high-latitudes (amplitude > 3 K). All variations are smaller over the seas due to the slower temperature changes over waters than lands. By using time-varying T_s-T_m models the estimated T_m 's RMSEs, which are also contoured in Fig. (5),
dropped significantly in the regions with large annual or diurnal variations.







210

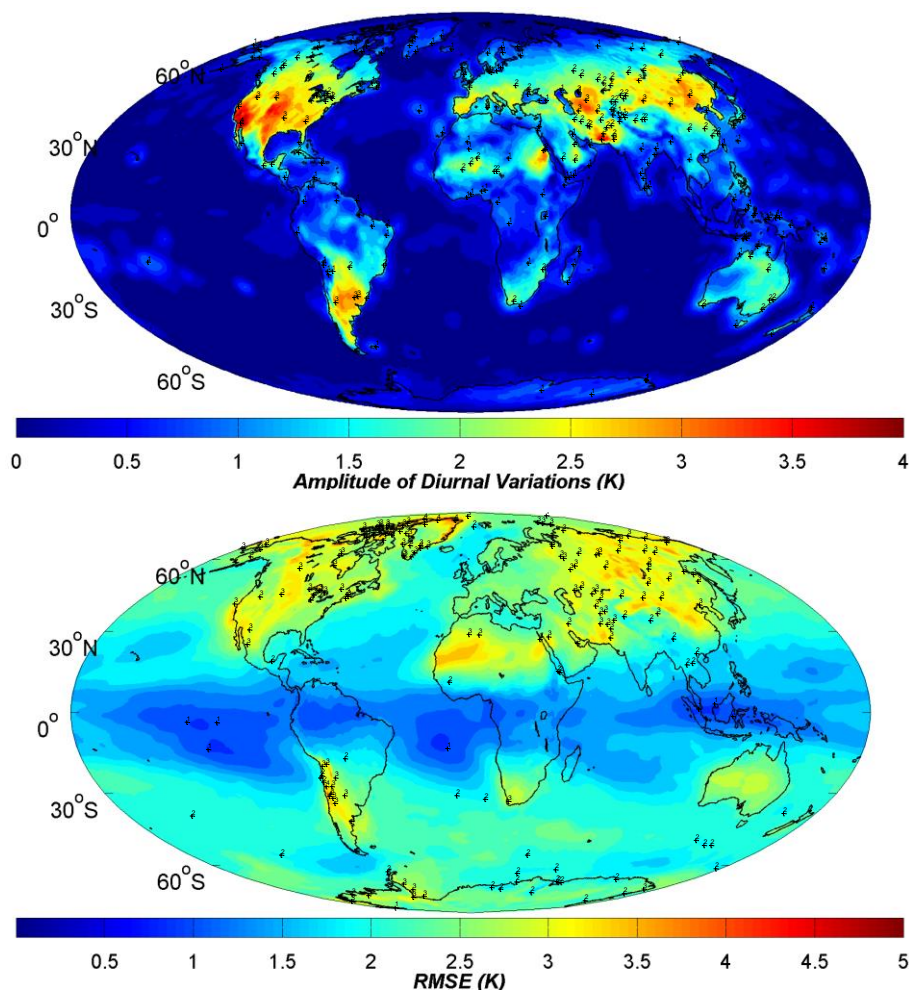


Figure 5: (top) slope constant a , (second) intercept constant b , amplitudes of T_m (third) annual, (forth) semiannual and (fifth) diurnal terms in our time-varying global gridded $T_s - T_m$ models, and (bottom) the model estimated T_m 's RMSE distribution.

4.3 Assessments of $T_s - T_m$ models

215

In order to assess the $T_s - T_m$ models precisions further using other independent data sources, we generated T_m and T_s from radiosonde data at 758 radiosonde stations in the year 2016. These data are not assimilated into 2009~2012 ERA-Interim datasets which we used in $T_s - T_m$ modeling process, so we can regard them as independent data to our model. At each radiosonde site, different $T_s - T_m$ models were employed to calculate T_m . Then these calculated T_m will be evaluated by comparisons with the integrated T_m values by radiosonde profiles (denoted as T_{m_RS}) twice a day.

220

We compared our $T_s - T_m$ models with other globally applied models in Tab. (1). The model estimated T_m are denoted as



T_{m_Bevis} , T_{m_LatR} , T_{m_static} and $T_{m_varying}$ respectively from Bevis equation, Yao's latitude-related model, our static global gridded model and time-varying global gridded model. The Lan's global gridded model(Lan et al., 2016) is replaced by our static global gridded model because of its much lower spatial resolution($4^\circ \times 5^\circ$) than our model ($0.75^\circ \times 0.75^\circ$). Actually Bevis model is established using regional radiosonde data so it should be a regional model, but it has been adopted in many other regional research so we regraded it as a global applicable equation. When global gridded models are employed, there is a problem that the radiosonde station always are not located at any grid node. Therefore the coefficients in T_s - T_m equations at radiosonde site's location should be horizontal interpolated from neighboring grids. The interpolation formula is expressed as (Jade and Vijayan, 2008):

$$C_{site} = \sum_{i=1}^4 w^i C_{grid}^i \quad (6)$$

C_{site} and C_{site}^i respectively represent the coefficients in T_s - T_m equations at radiosonde site location and its neighboring grids. w^i is the interpolation coefficients, which is determined using equation:

$$w^i = \frac{(R\psi^i)^{-\lambda}}{\sum_{j=1}^4 (R\psi^j)^{-\lambda}} \quad (7)$$

where $R=6378.17$ km is the mean radius of the earth, λ is the scale factor which equals one in our study, and ψ^i is the angular distance between the i th grid node and the station's position. ψ^i is computed using following formula related to latitude φ and longitude θ :

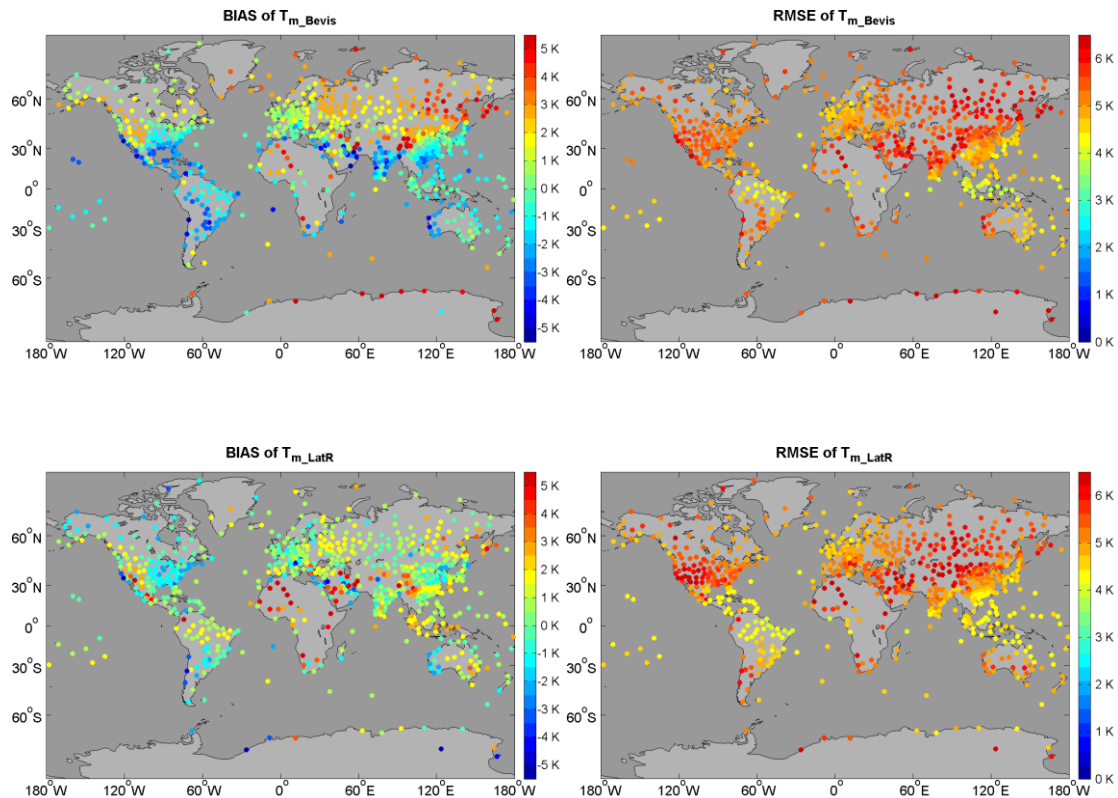
$$\cos \psi_i = \sin \varphi_i \cdot \sin \varphi + \cos \varphi_i \cdot \cos \varphi \cdot \cos(\theta_i - \theta) \quad (8)$$

Considering the reanalysis grids are definite and every radiosonde site is in situ, we can computed these interpolation coefficients in Eq. (6) for all radiosonde stations, then these coefficients are stored as constants to avoid reduplicate calculation.

Taking T_{m_RS} as reference values, we calculated the bias and root mean square error (RMSE) of T_{m_Bevis} , T_{m_LatR} , T_{m_static}

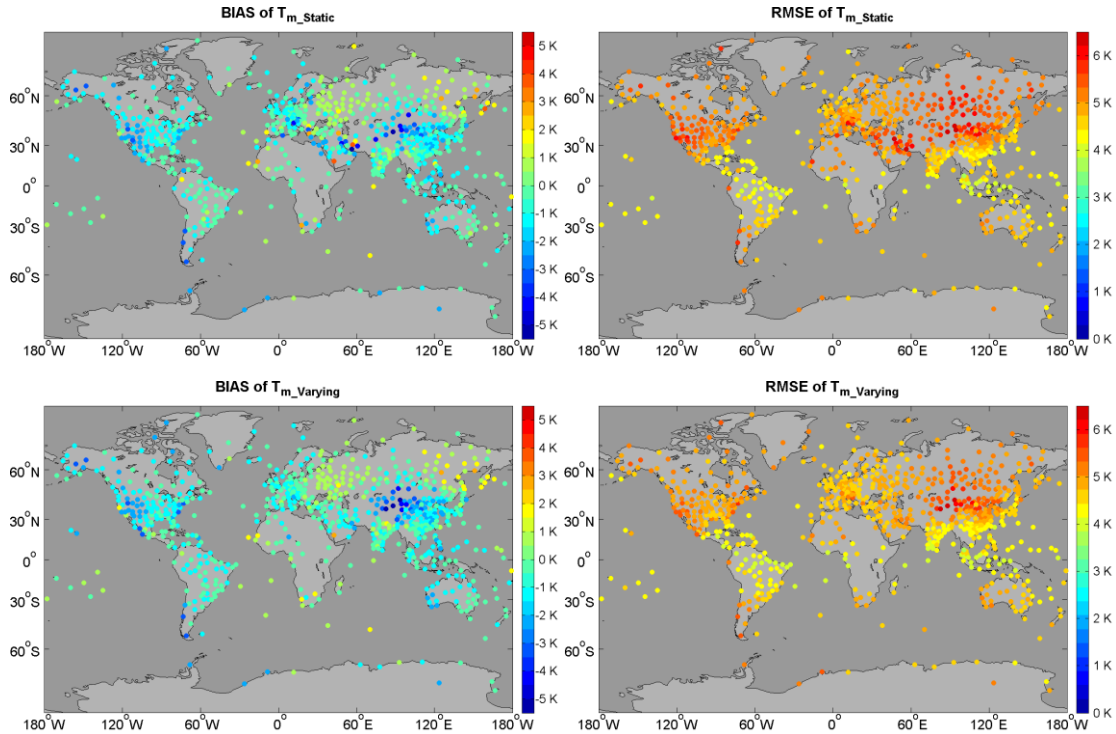


240 and $T_{m_varying}$ at each radiosonde site and illustrated them in Fig. (6). Obviously Bevis equation has bad precisions in many regions with absolute bias and RMSE larger than 5 K. T_{m_LatR} can reduce estimated biases in many regions, but the RMSEs remain large. And there still exist large biases at quite a few radiosonde stations, e.g. in the Africa or West Asia. T_{m_static} from the static global gridded model clearly remove large T_m biases at most of radiosonde stations and RMSEs also drop down evidently to less than 5 K. $T_{m_varying}$ perform better significantly all over the world, especially in the Middle East area, North
245 America or Siberia region, etc. Detailed statistics on the bias's and RMSE's distributions of different models are shown in Fig. (7) and Tab. (2). At over 96% radiosonde stations, biases of $T_{m_varying}$ are within -3~3 K and large positive biases (>3K) nearly disappear, while there are considerable large ones in T_{m_Bevis} and T_{m_LatR} . Improvements in RMSEs are more evidently. $T_{m_varying}$'s RMSEs are smaller than 4 K at over 90% radiosonde sites while few sites (<1%) have RMSEs larger than 5 K, which is clearly better than other models. In T_{m_Bevis} and T_{m_LatR} , there are more than 17% radiosonde sites have RMSE larger
250 than 5 K.



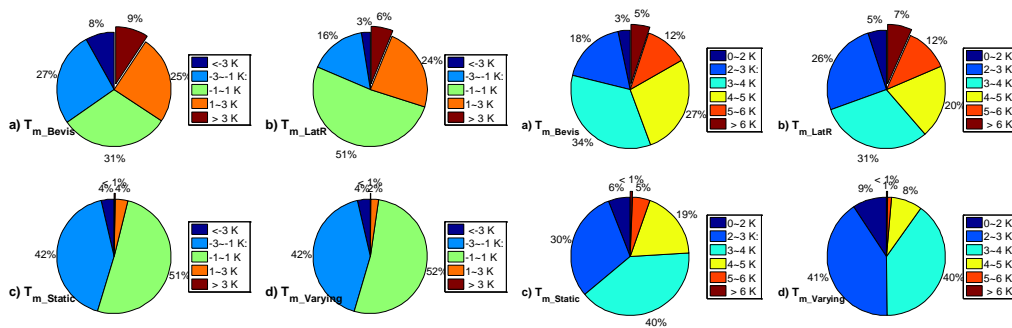


255



260

Figure 6: (left) bias and (right) RMSE of estimated T_m using T_s - T_m equations from (top) Bevis equation, (second) Yao's latitude-related model, (third) static global gridded model and (bottom) time-varying global gridded model at each radiosonde station comparing with radiosonde data of the year 2016.



1) Bias distribution

2) RMSE distribution

Figure 7: (left) bias's and (right) RMSE's distributions of T_{m_Bevis} , T_{m_LatR} , T_{m_static} and $T_{m_varying}$ compared with respect to radiosonde data at 758 stations in 2016

265

Table 2: Statistics of T_m estimates from different T_s - T_m models comparing with radiosonde T_m derivations



Statistics	T_{m_Bevis}	T_{m_LatR}	T_{m_static}	$T_{m_varying}$
Average value of absolute T_m bias (K)	1.90	1.31	1.17	1.13
Average value of T_m RMSE (K)	3.95	3.83	3.37	3.02
Average relative RMSE of T_m (%)	1.44	1.39	1.23	1.10
Max Relative RMSE of mean T_m (%)	3.69	4.26	2.57	2.40
% of sites with T_m RMSE < 4 K	55.67	61.35	75.86	90.11
% of sites with T_m Relative RMSE less than 1.5%	59.50	64.78	77.70	88.92

To verify the superior T_s - T_m model at each radiosonde site, we employed following statistical tests under the assumption of normal distribution of estimated T_m 's error:

(1) Firstly, Brown-Forsythe's tests (Brown and Forsythe, 1974) of equality of variances were carried out at each site for estimated T_m errors from two different models, e.g. model **A** and **B**. The purpose of this step is to determine that whether there is significant variance difference between two T_m results. If the test rejects the null hypothesis at 5% significance level that the errors of model **A** and **B** have the same variance, the model with smaller sample variance is regarded as the better one. However, if the test doesn't reject the homogeneity of variances, analysis of variance (ANOVA) is performed in the next step.

(2) ANOVA is a technique to analyze the differences among group means (Hogg, 1987). It evaluates the null hypothesis that the samples all have the same mean against the alternative that the means are not the same. If the null hypothesis is rejected at 5% significance level, the T_m sample with smaller absolute mean value is believed to be better. Otherwise we think that two models perform almost the same at this radiosonde site.

(3) After multiple tests and comparisons, the best model at each radiosonde stations may be determined. However, at some sites no superior model can be confirmed so all models are believed to have equivalent performances.

Finally we counted the number of sites at which each T_s - T_m model respectively performed superiorly, and the results are given in Tab. (3). At 634 radiosonde stations, which take 83.64% of all valid radiosonde sites, the time-varying global gridded model is superior to others, while other models are significantly better at only 10.82% of sites. It should be noticed that although T_{m_static} is not the best among the four models at all sites, it doesn't mean that T_{m_static} is "worse" than T_{m_Bevis} . Actually at most of sites T_{m_static} performs better than T_{m_Bevis} or T_{m_LatR} , but $T_{m_varying}$ is even better than T_{m_static} . Therefore it only reveals that at most of sites the precisions of static model are lower than time varying model.

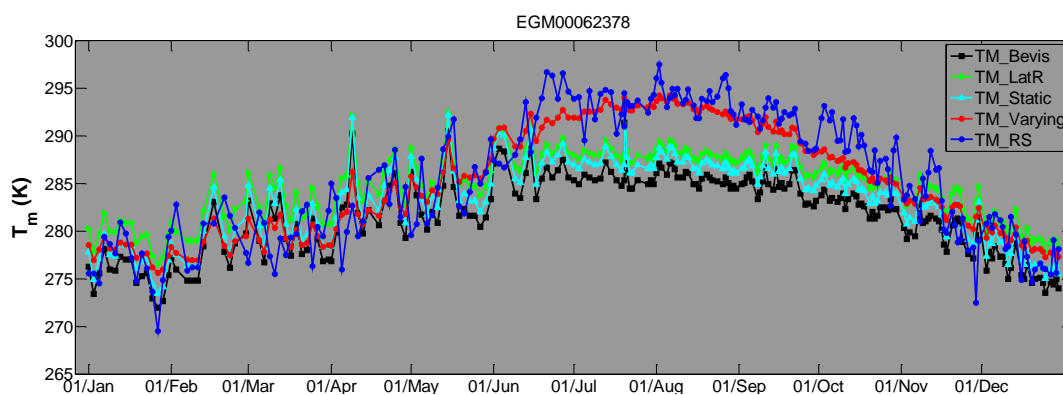


Table 3: Number of radiosonde sites at which the four global applied T_s - T_m models respectively perform superiorly

Superior model	None	T_{m_Bevis}	T_{m_LatR}	T_{m_static}	$T_{m_varying}$
Number of sites	42	63	19	0	634

In Fig. (8), T_m series at IGRA station NO.62378 (N29.8628°E31.3492°) are given. We can see that large negative biases (< -5 K) between T_{m_Bevis} (or T_{m_LatR}) and T_{m_RS} exist while T_{m_static} perform only slightly better from July to October. But $T_{m_varying}$ can eliminate most of the seasonal errors. Different properties of T_m series appear at another IGRA station NO.40841 (N30.2500°E56.9667°) shown in Fig. (8). Some observation data are missing but we can still see there are large positive differences (> 5 K) between T_{m_Bevis} (or T_{m_LatR}) and T_{m_RS} all through the year. T_{m_static} 's biases are much smaller than T_{m_Bevis} but still have some big errors in many months. The $T_{m_varying}$, however, still perform as well as at NO.62378 IGRA station, with small biases and good capturing of T_m 's variations.

On the other hand, even $T_{m_varying}$ also have large differences from T_{m_RS} at a few IGRA stations especially in Central Asia. It is because that our fitting analyses were based on the T_m values derived from reanalysis datasets, and reanalysis T_m did not agree well with radiosonde data at these IGRA sites during specific seasons. So improvements on reanalysis data in these region should be performed in future.



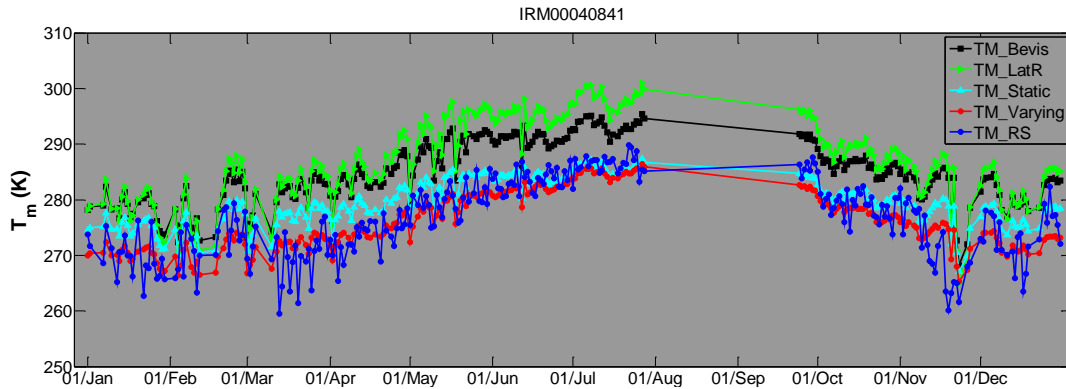


Figure 8: T_m series generated from Bevis equation (T_{m_Bevis}), Linear-related linear model (T_{m_LatR}), static global gridded T_s - T_m model (T_{m_static}), time-varying global gridded T_s - T_m model ($T_{m_varying}$) and radiosonde data (T_{m_RS}) at (top) EGM00062378 and (bottom) IRM00040841 IGRA sites.

5. GPS-PWV retrieving experiments

GPS-PWV has different error sources with different properties, including GPS ZWD error, surface temperature and pressure measurement errors, and T_m estimation error (Ning et al., 2016), etc. It is complicated to evaluate GPS-PWV uncertainty due to the lack of collaborated additional independent techniques to monitor water vapor at GPS site. Therefore several experiments were carried out to investigate GPS-PWV precisions carefully.

5.1 Impact of T_m estimation

In order to study to actual impacts of T_m on GPS-PWV retrievals, we firstly downloaded GPS ZTD products (Byun and Bar-Sever, 2009) at several IGS sites in the year 2016 from CDDIS FTP address (<ftp://cddis.gsfc.nasa.gov/pub/gps/products/troposphere/zpd>). These selected GPS sites were equipped with meteorological sensors so surface pressure and temperature measurements could be also obtained. $ZHDs$ were calculated using surface pressures and Saastamonien model and deducted from $ZTDs$ to obtain $ZWDs$. Then T_m were generated through five approaches: the first four T_m series were T_{m_Bevis} , T_{m_LatR} , T_{m_static} and $T_{m_varying}$, while the fifth T_m were integrated from ERA-Interim profiles and interpolated to GPS site locations (Wang et al., 2016). Finally, GPS-PWVs were generated from ZWD and five different T_m estimates. We denoted these GPS-PWV sets as PWV_{BTm} , PWV_{LTm} , PWV_{STm} , PWV_{VTm} and PWV_{ETm} . The only differences



between these GPS-PWVs are the T_m estimates, so impacts of other errors could be excluded.

Because the T_m from ERA-Interim is believed to be the most accurate, so we regarded the PWV_{ETm} as reference values to
 320 assess other PWVs. Finally PWVs at 74 IGS sites which have over one hundred compared points were obtained. The relative
 RMSEs of PWV_{BTm} , PWV_{LTm} , PWV_{STm} and PWV_{VTm} at these selected stations were calculated and illustrated in Fig. (9), and
 detailed statistics are given in Tab. (4). Mean relative error of all sites drops from 1.18% of PWV_{BTm} to 0.91% of PWV_{VTm} .
 Obviously at most sites PWV_{VTm} , which have minim relative errors, are prior to other PWV retrievals. At 62 sites PWV_{VTm}
 obtain relative RMSE smaller than 1.0%, while at only 28 sites PWV_{BTm} perform similarly and 31 sites of PWV_{LTm} . Some
 325 relative RMSEs were remarkably reduced. For example, at ALIC site which located in Australia with mean PWV of about 23
 mm, the relative RMSE dropped from 1.97% of PWV_{BTm} to 1.10% of PWV_{VTm} . The time series of relative differences of
 PWV_{BTm} , PWV_{LTm} , PWV_{STm} and PWV_{VTm} at ALIC station are given in Fig. (10). Obviously PWV_{BTm} and PWV_{LTm} have bigger
 relative errors although the year while PWV differences are evidently larger only in summer season. It is attributed to the
 wetter atmosphere in summer than in winter. PWV_{STm} eliminate those large differences but still retain some residual errors,
 330 which are removed more than 1.0 mm in PWV_{VTm} further. All these results demonstrate that our time-varying global gridded
 has precision advantages.

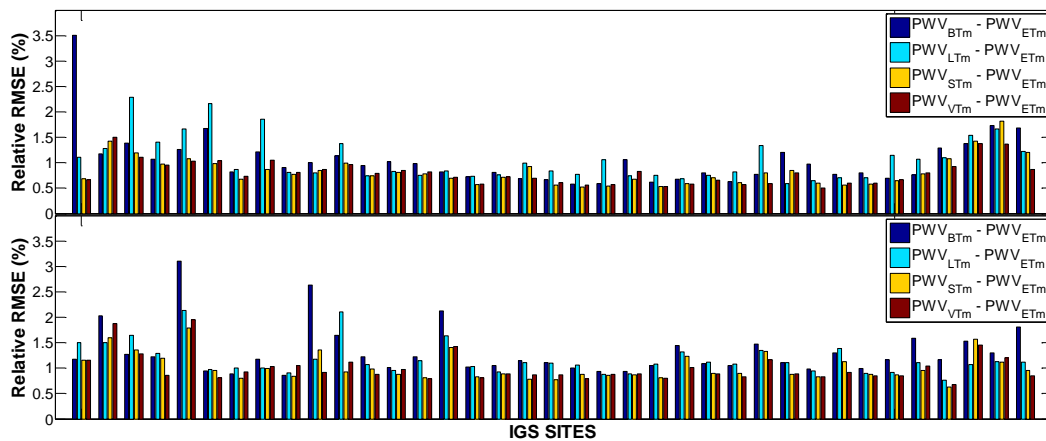


Figure 9: Relative RMSEs of PWV_{BTm} , PWV_{STm} and PWV_{VTm} compared with PWV_{ETm} at 74 IGS stations in the year 2016

Table 4: Statistics about relative errors of different PWV retrievals

Statistics	PWV_{BTm}	PWV_{LTm}	PWV_{STm}	PWV_{VTm}
------------	-------------	-------------	-------------	-------------



Mean relative RMSE of all sites	1.18%	1.12%	0.93%	0.91%
Number of sites with relative errors < 1.0%	28	31	55	62

335

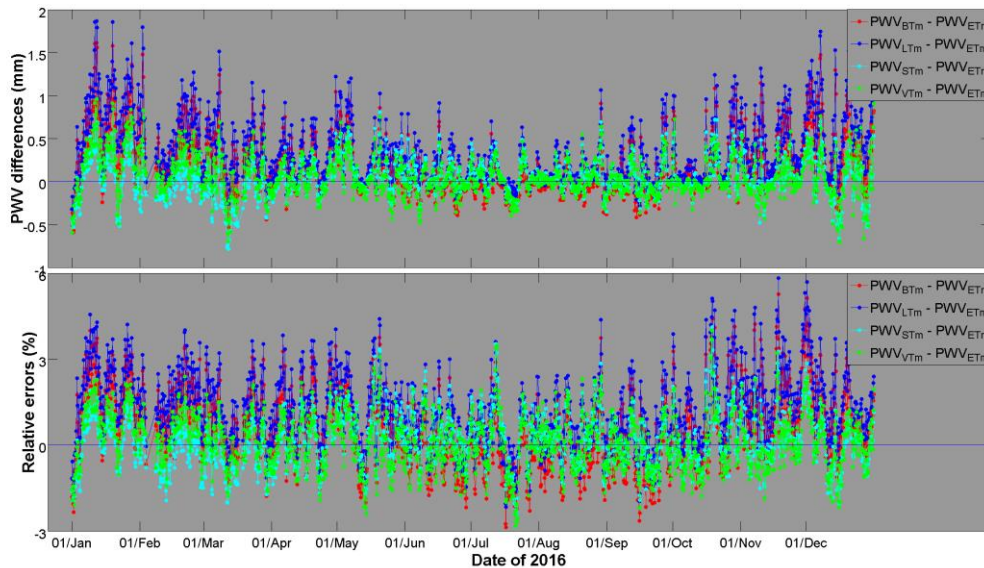


Figure 10: (top) PWV differences and (bottom) relative differences of PWV_{BTm} , PWV_{LTm} , PWV_{STm} and PWV_{VTm} compared with PWV_{ETm} at ALIC station in the year 2016.

5.2 Comparisons between GPS-PWVs and radiosonde PWVs

340

Among our selected 74 IGS sites, there are only 11 sites located within 5 km to nearby IGRA radiosonde stations. At these common stations, we generated PWVs from radiosonde data (PWV_{RS}) by adjusting sounding profiles to the heights of IGS sites. It worth noticing that geoid undulation corrections should be carried out on each IGS site's geoid height (Jiang et al., 2016). Then we compared PWV_{BTm} , PWV_{LTm} , PWV_{STm} , PWV_{VTm} and PWV_{ETm} with PWV_{RS} . Statistics are shown in Fig.

345

(11). The RMSEs of GPS-PWVs are around 1~5 mm. Comparisons indicate that at most selected sites the RMSEs of different GPS-PWV retrievals are very close (differences < 0.2 mm) regardless of the T_m sources applied, which means that other errors (e.g. ZTD estimation errors or sounding sensors errors) instead of T_m occupied the differences between GPS-PWVs and radiosonde PWVs. However, we still found obvious gaps between PWVs at NRIL (N88.3598° E69.3618° , 4.1km to nearby radiosonde NO.23078 sites). RMSEs decrease from 2.29 mm of PWV_{BTm} to 1.84mm of PWV_{VTm} and 1.42 mm of PWV_{ETm} . As shown in Fig. (12), the large PWV differences mainly appeared from May to September. During such five months, mean



350 GPS-PWV differences to PWV_{RS} decreased by over 30% from 2.52 mm of PWV_{BTm} to 1.67 mm of PWV_{VTm} .

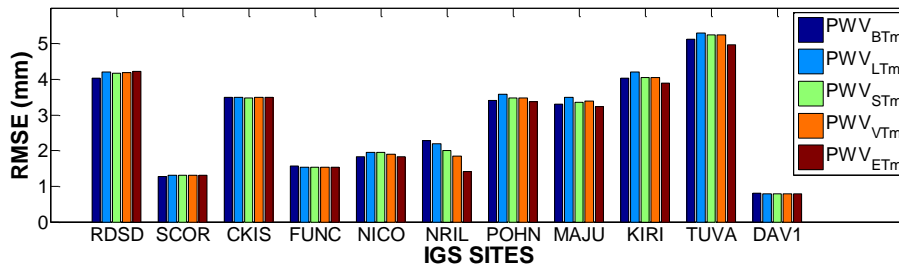


Figure 11: RMSEs of PWV_{BTm} , PWV_{STm} , PWV_{VTm} and PWV_{ETm} compared with PWV_{RS} at 11 IGS stations in the year 2016

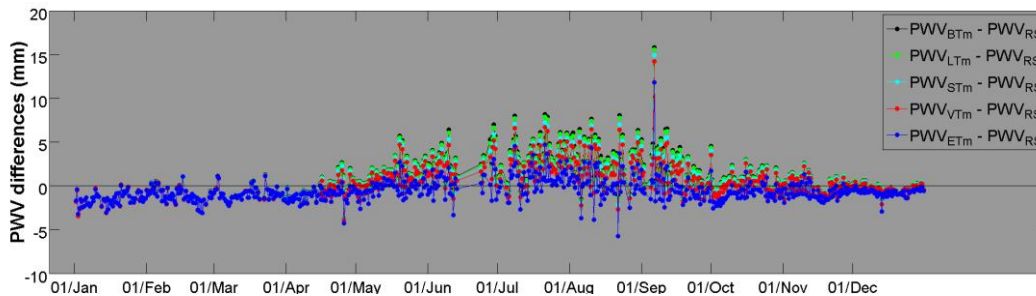


Figure 12: PWV differences of PWV_{BTm} , PWV_{LTm} , PWV_{STm} , PWV_{VTm} and PWV_{ETm} compared with PWV_{RS} at NIRL station in the year 2016

355

6. Summary and conclusion

In this study, we estimated T_m using temperature and humidity profile data from IGRA radiosonde data and ERA-Interim reanalysis datasets over a four-years-long period from year 2009 to 2012. Surface air temperature T_s were also extracted from the two data sets. Then we analyzed the relationship between T_s and T_m at each grid node of reanalysis data and radiosonde station. Analyses indicated that: (1) T_m has stronger relationship with T_s in mid-high latitudes than in low latitudes; (2) In low latitudes, T_s - T_m correlation coefficients are higher over lands than over oceans; (3) the T_s - T_m relationship's variation properties is much more complicated rather than only dependence on point's latitude, and (4) T_s - T_m relation has strong annual, semiannual and diurnal variations in many areas.

360

365

Using global gridded ERA-Interim datasets from 2009 to 2012, we developed static and time-varying global gridded T_s - T_m models. Annual, semiannual and diurnal variations in T_s - T_m relationship are considered in time-varying model. Then we



370 evaluated T_m results from different T_s - T_m models by comparing them with radiosonde data in 2016. Results demonstrate time-varying global gridded T_s - T_m model has significant global precision advantage over other global applied models. Average T_m RMSE reduces by about 1 K. The proportion of sites with small biases and RMSEs increases significantly. At over 90% radiosonde sites, time-varying global gridded model has RMSE smaller than 4 K, and the RMSEs larger than 5 K nearly disappear, while by applying Bevis or latitude-related models there are more than 17% radiosonde sites have RMSEs larger than 5 K. Multiple statistical tests at 5% significance level verify the significant superiority of the new time-varying model at more than 83.64% of radiosonde sites, while other three models are obviously better at only 10.82% of sites. Analyses at specific stations also demonstrate that time-varying global model can eliminate large errors in estimated T_m series.

375 More precise T_s - T_m models also have positive impacts on GPS-PWV retrievals. Regarding the GPS-PWVs using ERA-Interim T_m estimates as references, relative errors of GPS-PWV using time-varying global gridded T_s - T_m models are within 1.0% at more than 83% of IGS sites, which is much more than other models. The differences between GPS-PWVs and radiosonde PWVs are around 1~5 mm and mainly influenced by comprehensive error sources rather than single T_m . But at special site, such differences could decrease by more than 30% in wetter conditions.

380 According to our experiments, we are confident that the time-varying global gridded T_s - T_m models presented here will help us to retrieve GPS PWV more precisely, or to study precise PWV variations in high temporal resolution as well as T_s observations which is much greater than of conventional reanalysis datasets (6 hours) or radiosonde data (12 hours). Matlab array file consisting of global gridded coefficients in our model, as well as Matlab codes to interpolate coefficients to any given location, are provided as the supplements of this study. It is convenient to use for researchers and applicants in relevant fields.

385 *Data sets*

Radiosonde data: <ftp://ftp.ncdc.noaa.gov/pub/data/igra>

ERA-Interim Project: <https://doi.org/10.5065/D6CR5RD9>

GPS-ZTD Product: <ftp://cddis.gsfc.nasa.gov/pub/gps/products/troposphere/zpd>

390



Acknowledgments

This study is supported by National Natural Science Foundation of China (No. 41604028), the Anhui Provincial Natural Science Foundation (No. 1708085QD83), and the Doctoral Research Start-up Funds Projects of Anhui University (No. J01001966). The authors thank European Centre for Medium-Range Weather Forecasts for providing the ERA-Interim dataset. We also thank the National Centers for Environmental Information for the IGRA datasets and International GNSS Service for the GNSS troposphere products.

395

Competing interests

The authors declare that they have no conflict of interest.

400



References

- Adams, D. K., Barbosa, H. M. J., and De Los Rios, K. P. G.: A Spatiotemporal Water Vapor-Deep Convection Correlation Metric Derived from the Amazon Dense GNSS Meteorological Network, *Monthly Weather Review*, 145, 279-288, 10.1175/mwr-d-16-0140.1, 2017.
- Adler, B., Kalthoff, N., Kohler, M., Handwerker, J., Wieser, A., Corsmeier, U., Kottmeier, C., Lambert, D., and Bock, O.: The variability of water vapour and pre-convective conditions over the mountainous island of Corsica, *Quarterly Journal Of the Royal Meteorological Society*, 142, 335-346, 10.1002/qj.2545, 2016.
- Bevis, M., Businger, S., Herring, T. A., Rocken, C., Anthes, R. A., and Ware, R. H.: GPS meteorology: Remote sensing of atmospheric water vapor using the global positioning system, *Journal of Geophysical Research: Atmospheres*, 97, 15787-15801, 10.1029/92JD01517, 1992.
- Bohm, J., Moller, G., Schindelegger, M., Pain, G., and Weber, R.: Development of an improved empirical model for slant delays in the troposphere (GPT2w), *Gps Solutions*, 19, 433-441, 10.1007/s10291-014-0403-7, 2015.
- Brown, M. B., and Forsythe, A. B.: Robust Tests for the Equality of Variances, *Publications of the American Statistical Association*, 69, 364-367, 1974.
- Byun, S. H., and Bar-Sever, Y. E.: A new type of troposphere zenith path delay product of the international GNSS service, *J. Geodesy*, 83, 367-373, 10.1007/s00190-008-0288-8, 2009.
- Campmany, E., Bech, J., Rodriguez-Marcos, J., Sola, Y., and Lorente, J.: A comparison of total precipitable water measurements from radiosonde and sunphotometers, *Atmospheric Research*, 97, 385-392, 10.1016/j.atmosres.2010.04.016, 2010.
- Chen, P., Yao, W. Q., and Zhu, X. J.: Realization of global empirical model for mapping zenith wet delays onto precipitable water using NCEP re-analysis data, *Geophys. J. Int.*, 198, 1748-1757, 10.1093/gji/ggu223, 2014.
- Ciesielski, P. E., Chang, W. M., Huang, S. C., Johnson, R. H., Jou, B. J. D., Lee, W. C., Lin, P. H., Liu, C. H., and Wang, J. H.: Quality-Controlled Upper-Air Sounding Dataset for TIMREX/SoWMEX: Development and Corrections, *Journal Of Atmospheric And Oceanic Technology*, 27, 1802-1821, 10.1175/2010jtecha1481.1, 2010.
- Haase, J., Ge, M., Vedel, H., and Calais, E.: Accuracy and variability of GPS tropospheric delay measurements of water vapor in the western Mediterranean, *Journal of Applied Meteorology*, 42, 1547-1568, 10.1175/1520-0450(2003)042<1547:AAVOGT>2.0.CO;2, 2003.
- Hogg, R. V., and Ledolter, J.: *Engineering Statistics*, Macmillan, New York, 1987.
- Jade, S., and Vijayan, M. S. M.: GPS-based atmospheric precipitable water vapor estimation using meteorological parameters interpolated from NCEP global reanalysis data, *Journal of Geophysical Research-Atmospheres*, 113, 10.1029/2007jd008758, 2008.
- Jiang, P., Ye, S. R., Chen, D. Z., Liu, Y. Y., and Xia, P. F.: Retrieving Precipitable Water Vapor Data Using GPS Zenith Delays and Global Reanalysis Data in China, *Remote Sensing*, 8, 10.3390/rs8050389, 2016.
- Karabatic, A., Weber, R., and Haiden, T.: Near real-time estimation of tropospheric water vapour content from ground based GNSS data and its potential contribution to weather now-casting in Austria, *Adv. Space Res.*, 47, 1691-1703, 10.1016/j.asr.2010.10.028, 2011.



- Kealy, J., Foster, J., and Businger, S.: GPS meteorology: An investigation of ocean-based precipitable water estimates, *Journal Of Geophysical Research-Atmospheres*, 117, 10.1029/2011jd017422, 2012.
- 440 Lan, Z., Zhang, B., and Geng, Y.: Establishment and analysis of global gridded Tm – Ts relationship model, *Geodesy and Geodynamics*, 7, 101-107, <https://doi.org/10.1016/j.geog.2016.02.001>, 2016.
- Lee, J., Park, J.-U., Cho, J., Baek, J., and Kim, H. W.: A characteristic analysis of fog using GPS-derived integrated water vapour, *Meteorological Applications*, 17, 463-473, 10.1002/met.182, 2010.
- Li, X., Zhang, L., Cao, X. J., Quan, J. N., Wang, T. H., Liang, J. N., and Shi, J. S.: Retrieval of precipitable water vapor using MFRSR and comparison with other multisensors over the semi-arid area of northwest China, *Atmospheric Research*, 172, 83-94, 445 10.1016/j.atmosres.2015.12.015, 2016.
- Liu, Z. Z., Li, M., Zhong, W. K., and Wong, M. S.: An approach to evaluate the absolute accuracy of WVR water vapor measurements inferred from multiple water vapor techniques, *Journal Of Geodynamics*, 72, 86-94, 10.1016/j.jog.2013.09.002, 2013.
- Lu, C. X., Li, X. X., Nilsson, T., Ning, T., Heinkelmann, R., Ge, M. R., Glaser, S., and Schuh, H.: Real-time retrieval of precipitable 450 water vapor from GPS and BeiDou observations, *J. Geodesy*, 89, 843-856, 10.1007/s00190-015-0818-0, 2015.
- Mahoney, K., Jackson, D. L., Neiman, P., Hughes, M., Darby, L., Wick, G., White, A., Sukovich, E., and Cifelli, R.: Understanding the role of atmospheric rivers in heavy precipitation in the Southeast US, *Monthly Weather Review*, 10.1175/MWR-D-15-0279.1, 2016.
- Means, J. D.: GPS Precipitable Water as a Diagnostic of the North American Monsoon in California and Nevada, *J. Clim.*, 26, 455 1432-1444, 10.1175/jcli-d-12-00185.1, 2013.
- Ning, T., Wang, J., Elgered, G., Dick, G., Wickert, J., Bradke, M., Sommer, M., Querel, R., and Smale, D.: The uncertainty of the atmospheric integrated water vapour estimated from GNSS observations, *Atmos. Meas. Tech.*, 9, 79-92, 10.5194/amt-9-79-2016, 2016.
- Pacione, R., and Vespe, F.: Comparative studies for the assessment of the quality of near-real-time GPS-derived atmospheric 460 parameters, *Journal of Atmospheric and Oceanic Technology*, 25, 701-714, 10.1175/2007jtecha935.1, 2008.
- Perez-Ramirez, D., Whiteman, D. N., Smirnov, A., Lyamani, H., Holben, B. N., Pinker, R., Andrade, M., and Alados-Arboledas, L.: Evaluation of AERONET precipitable water vapor versus microwave radiometry, GPS, and radiosondes at ARM sites, *Journal Of Geophysical Research-Atmospheres*, 119, 9596-9613, 10.1002/2014jd021730, 2014.
- Raju, C. S., Saha, K., Thampi, B. V., and Parameswaran, K.: Empirical model for mean temperature for Indian zone and 465 estimation of precipitable water vapor from ground based GPS measurements, *Ann. Geophys.*, 25, 1935-1948, 2007.
- Rocken, C., Johnson, J., Van Hove, T., and Iwabuchi, T.: Atmospheric water vapor and geoid measurements in the open ocean with GPS, *Geophysical Research Letters*, 32, 10.1029/2005gl022573, 2005.
- Rohm, W., Yuan, Y. B., Biadegligne, B., Zhang, K. F., and Le Marshall, J.: Ground-based GNSS ZTD/IWV estimation system for numerical weather prediction in challenging weather conditions, *Atmospheric Research*, 138, 414-426, 470 10.1016/j.atmosres.2013.11.026, 2014.
- Saastamoinen, J.: Atmospheric correction for the troposphere and stratosphere in radio ranging of satellites, *Use of Artificial Satellites for Geodesy*, 15, 274-251, 1972.
- Sheng, P., Mao, J., Li, J., Ge, Z., Zhang, A., Sang, J., Pan, N., and Zhang, H.: *Atmospheric Physics 2ed.*, Peking University Press,



- Beijing, 2013.
- 475 Singh, D., Ghosh, J. K., and Kashyap, D.: Weighted mean temperature model for extra tropical region of India, *Journal of Atmospheric and Solar-Terrestrial Physics*, 107, 48-53, <http://dx.doi.org/10.1016/j.jastp.2013.10.016>, 2014.
- Song, J. J., Wang, Y., and Tang, J. P.: A Hiatus of the Greenhouse Effect, *Sci Rep*, 6, 9, 10.1038/srep33315, 2016.
- Van Baelen, J., and Penide, G.: Study of water vapor vertical variability and possible cloud formation with a small network of GPS stations, *Geophysical Research Letters*, 36, 10.1029/2008gl036148, 2009.
- 480 Wang, J. H., Zhang, L. Y., and Dai, A.: Global estimates of water-vapor-weighted mean temperature of the atmosphere for GPS applications, *Journal of Geophysical Research-Atmospheres*, 110, 10.1029/2005jd006215, 2005.
- Wang, X. M., Zhang, K. F., Wu, S. Q., Fan, S. J., and Cheng, Y. Y.: Water vapor-weighted mean temperature and its impact on the determination of precipitable water vapor and its linear trend, *Journal Of Geophysical Research-Atmospheres*, 121, 833-852, 10.1002/2015jd024181, 2016.
- 485 Wang, X. Y., Song, L. C., and Cao, Y. C.: Analysis of the weighted mean temperature of china based on sounding and ECMWF reanalysis data, *Acta Meteorol. Sin.*, 26, 642-652, 10.1007/s13351-012-0508-2, 2012.
- Yao, Y., Zhang, B., Xu, C., and Yan, F.: Improved one/multi-parameter models that consider seasonal and geographic variations for estimating weighted mean temperature in ground-based GPS meteorology, *J. Geodesy*, 88, 273-282, 10.1007/s00190-013-0684-6, 2014a.
- 490 Yao, Y. B., Zhu, S., and Yue, S. Q.: A globally applicable, season-specific model for estimating the weighted mean temperature of the atmosphere, *J. Geodesy*, 86, 1125-1135, 10.1007/s00190-012-0568-1, 2012.
- Yao, Y. B., Zhang, B., Xu, C. Q., and Chen, J. J.: Analysis of the global T(m)-T(s) correlation and establishment of the latitude-related linear model, *Chinese Science Bulletin*, 59, 2340-2347, 10.1007/s11434-014-0275-9, 2014b.